

## 8 Photonic Crystals and Metamaterials

**Highlights of this chapter:** In this chapter we discuss photonic crystals as a special class of structured dielectric materials with novel optical properties. We provide the basic theoretical concepts and provide examples for applications. In the last part we introduce and discuss metamaterials as a more general concept of artificial optical materials with novel properties.

### 8.1 Introduction

In free space there is a simple relation between the frequency  $f$ , the wavelength  $\lambda$ , and the vacuum speed of light  $c_0$ :

$$c_0 = \lambda f \quad (348)$$

or

$$\omega = c_0 k \quad (349)$$

for the wave vector  $k = 2\pi/\lambda$ .

This relation is the *dispersion relation* for the electromagnetic field in vacuum.

In an isotropic, homogeneous medium with an index of refraction  $n$  one finds an identical dispersion relation if  $c_0$  is replaced by  $c = c_0/n$ :

$$\omega = ck \quad (350)$$

An important quantity when describing the interaction of light and matter is the *Density of States* (DOS).

In free space the DOS is proportional to  $\omega^2$ :

$$D(\omega) = \frac{\omega^2 V}{\pi^2 c^3} \quad (351)$$

where  $V$  is a volume element.

For example, the spontaneous emission rate is proportional to the density of states, i.e., if the DOS is changed then the spontaneous emission is modified as well.

*Photonic Crystals* or *Photonic Bandgap Materials* are materials with a periodic modulation of the index of refraction. The period of the modulation is typically on the order of the wavelength  $\lambda/2$ , which is some 100 nm in the visible.

Modulation can occur in one, two, or all three spatial dimensions (s. figure 202).

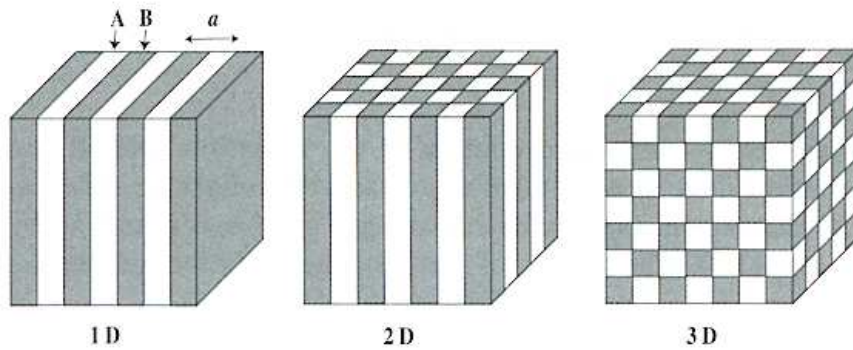


Figure 202: Modulation of the index of refraction in a photonic crystal structure in one, two, and three dimensions. [from Sakoda "Optical Properties of Photonic Crystals"]

The modulation of the index of refraction changes the dispersion relation and the DOS in an essential way. The following figure 203 shows the DOS in free space and in a one-dimensional photonic crystal:

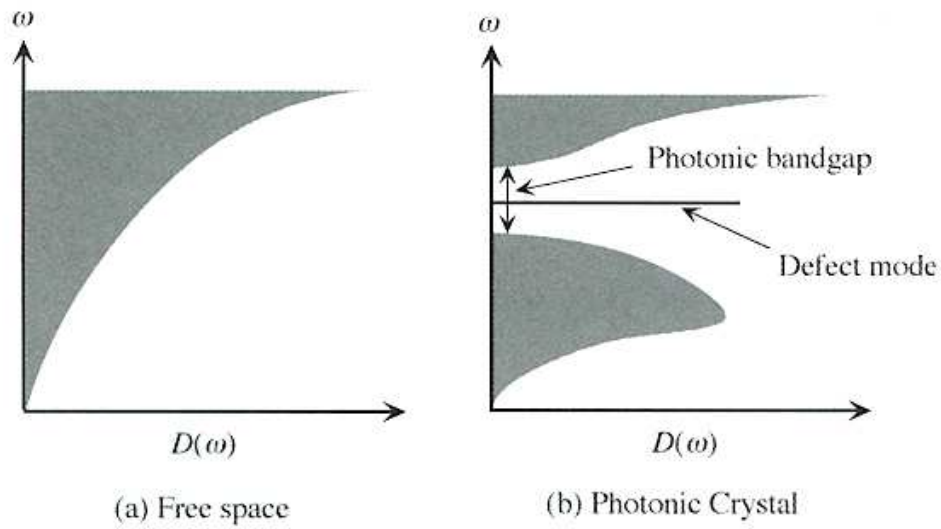


Figure 203: DOS in free space and in a photonic crystal. [from Sakoda "Optical Properties of Photonic Crystals"]

An example for a one-dimensional Photonic Bandgap Material is a Bragg reflector (see figures 204 and 205). In a Bragg-reflector, jumps of the optical phase after reflection or transmission of a wave lead to constructive (reflection) and destructive (transmission) interference.

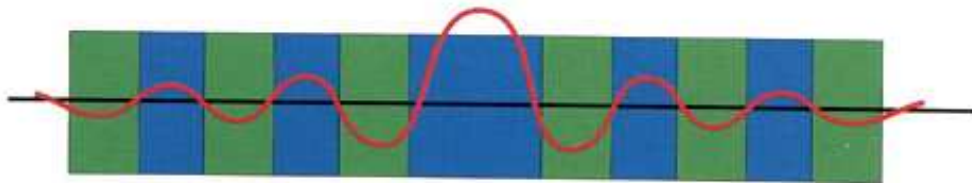


Figure 204: Schematics of a resonator formed by two Bragg mirrors and calculated intensity distribution. [from Joannopoulos "Photonic Crystals"]

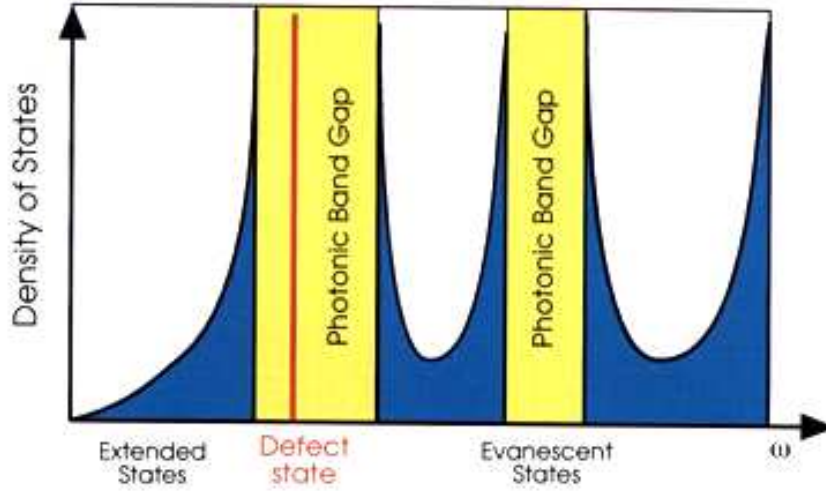


Figure 205: DOS of a Bragg resonator. [from Joannopoulos "Photonic Crystals"]

Bragg-reflectors can be fabricated by thin-film technology, e.g., molecular beam epitaxy, and are widely used as mirrors, e.g., in VCSELs (vertical cavity surface emitting laser). Figure 206 shows an SEM image of a VCSEL.

## 8.2 Maxwell's equation as eigenvalue problem

In order to calculate the optical properties of photonic crystals one starts with the source-free Maxwell's equations:

$$\nabla \times E(r, t) = -\frac{\partial B(r, t)}{\partial t} \quad (352)$$

$$\nabla \times H(r, t) = \frac{\partial D(r, t)}{\partial t} \quad (353)$$

$$\nabla \cdot D(r, t) = 0 \quad (354)$$

$$\nabla \cdot B(r, t) = 0 \quad (355)$$

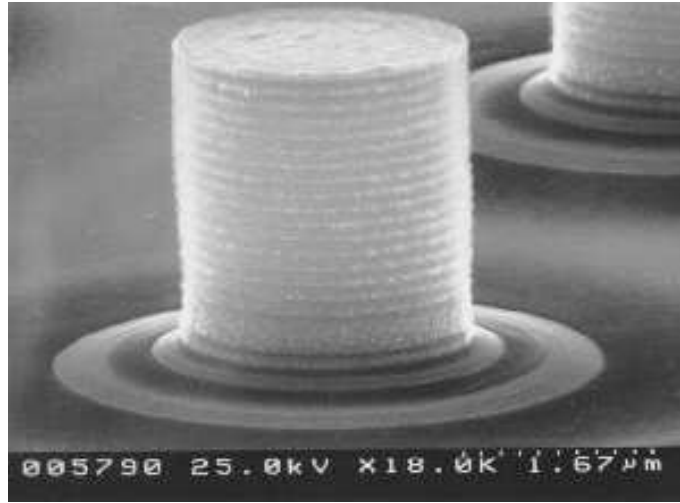


Figure 206: SEM-image of a Bragg mirror on a VCSEL.

where  $E$  is the electric field,  $D$  the dielectric displacement,  $H$  the magnetic field, and  $B$  the magnetic induction.

In a linear medium it is:

$$D(r, t) = \epsilon_0 \epsilon(r) E(r, t) \quad (356)$$

$$H(r, t) = \mu_0^{-1} B(r, t) \quad (357)$$

As already shown in the theory paper inserting into Maxwell's equation and separating  $E(r, t)$  and  $H(r, t)$  results in the homogeneous wave equations:

$$\frac{1}{\epsilon(r)} \nabla \times \{ \nabla \times E(r, t) \} + \frac{1}{c^2} \frac{\partial^2 E(r, t)}{\partial t^2} = 0 \quad (358)$$

$$\nabla \times \left\{ \frac{1}{\epsilon(r)} \nabla \times H(r, t) \right\} + \frac{1}{c^2} \frac{\partial^2 H(r, t)}{\partial t^2} = 0 \quad (359)$$

with

$$c = \frac{1}{\sqrt{\epsilon_0 \mu_0}} \quad (360)$$

For a harmonic time dependence

$$E(r, t) = E(r)e^{-i\omega t} \quad (361)$$

$$H(r, t) = H(r)e^{-i\omega t} \quad (362)$$

inserting in equation 358 provides the **eigenvalue problem**:

$$L_E E(r) = \frac{1}{\epsilon(r)} \nabla \times \{ \nabla \times E(r) \} = \frac{\omega^2}{c^2} E(r) \quad (363)$$

$$L_H H(r) = \nabla \times \left\{ \frac{1}{\epsilon(r)} \nabla \times H(r) \right\} = \frac{\omega^2}{c^2} H(r) \quad (364)$$

In a photonic crystal the dielectric constant  $\epsilon(r)$  is a periodic function:

$$\epsilon(r + a_i) = \epsilon(r) \quad (365)$$

where  $\{a_i\}$  are lattice vectors of a unit cell.

If one defines also the reciprocal elementary lattice vectors  $\{b_i\}$  and the reciprocal lattice vector  $G$ :

$$a_i b_j = 2\pi \delta_{ij} \quad (366)$$

$$G = l_1 b_1 + l_2 b_2 + l_3 b_3 \quad (367)$$

then  $\epsilon^{-1}(r)$  can be written as a Fourier series as follows:

$$\epsilon^{-1}(r) = \sum_G \kappa(G) \exp(iGr) \quad (368)$$

with

$$\kappa(-G) = \kappa^*(G) \quad (369)$$

if  $\epsilon$  is real.

Now the solutions of the Maxwell equation are also periodic and the *Bloch-Theorem* applies in analogy to *wavefunctions of electrons in a crystal*, i.e.,  $E(r)$  and  $H(r)$  are characterized by a wave vector  $k$  within the first Brillouin zone and a band index  $n$ :

$$E(r) = E_{kn}(r) = u_{kn}(r)e^{ikr} \quad (370)$$

$$H(r) = H_{kn}(r) = v_{kn}(r)e^{ikr} \quad (371)$$

where  $u_{kn}(r)$  and  $v_{kn}(r)$  are periodic:

$$u_{kn}(r + a_i) = u_{kn}(r) \quad (372)$$

$$v_{kn}(r + a_i) = v_{kn}(r) \quad \text{für } i = 1, 2, 3 \quad (373)$$

Similar as  $\epsilon^{-1}(r)$  also  $E_{kn}(r)$  and  $H_{kn}(r)$  can be represented as a Fourier series:

$$E_{kn}(r) = \sum_G E_{kn}(G) \exp(i(k + G)r) \quad (374)$$

$$H_{kn}(r) = \sum_G H_{kn}(G) \exp(i(k + G)r) \quad (375)$$

Inserting into the wave equations 363 finally gives the equations:

$$-\sum_{G'} \kappa(G - G')(k + G') \times \{(k + G') \times E_{kn}(G')\} = \frac{\omega_{kn}^2}{c^2} E_{kn}(G) \quad (376)$$

$$-\sum_{G'} \kappa(G - G')(k + G) \times \{(k + G') \times H_{kn}(G')\} = \frac{\omega_{kn}^2}{c^2} H_{kn}(G) \quad (377)$$

These equations have to be solved numerically, i.e., the summation is truncated at a specific  $G'$  and for each  $k$  the matrix is diagonalized.

The solutions provide the dispersion relation and the band structure of the photonic crystal.

The expansion in plane waves (Fourier series) converges only weakly in general. For different geometries a more appropriate basis set can be chosen, e.g., cylinder or spherical functions.

## Symmetries

The solutions of the equations above have two interesting symmetries:

1. If a length scaling is introduced

$$\frac{1}{a}(r) = r' \quad \text{and} \quad \frac{c}{a}t = t' \quad (378)$$

then for the scaled quantities

$$\epsilon_{sc}(r') = \epsilon(r) \quad \text{and} \quad (379)$$

$$E_{sc}(r', t') = E(r, t) \quad (380)$$

the scaled wave equation holds

$$\frac{1}{\epsilon'(r')} \nabla' \times \{ \nabla' \times E_{sc}(r', t') \} + \frac{1}{c^2} \frac{\partial^2 E_{sc}(r', t')}{\partial t'^2} = 0 \quad (381)$$

The dispersion relation  $\omega' = \omega'(k')$  with scaled

$$\omega' = \frac{a}{2\pi c} \omega \quad (382)$$

$$k' = \frac{a}{2\pi} k \quad (383)$$

is universal.

This means experiments can be performed, e.g., with microwaves to find out the dispersion relations for a scaled photonic crystal in the visible.

2. The second symmetry results from time reversal symmetry: One finds easily that if  $E_{tr}(r, t')$  with

$$t' = -t \quad (384)$$

$$E_{tr}(r, t') = E(r, -t) \quad (385)$$

is a solution of the wave equation

$$\frac{1}{\epsilon(r)} \nabla \times \{ \nabla \times E_{tr}(r, t') \} + \frac{1}{c^2} \frac{\partial^2 E_{tr}(r, t')}{\partial t'^2} = 0 \quad (386)$$

then:

$$\omega_{-kn} = \omega_{kn} \quad (387)$$

$$u_{-kn}(r) = u_{kn}^*(r) \quad (388)$$

i.e. the dispersion relation has *inversion symmetry*.

### 8.3 Photonic Bandgaps in one dimension

A simple example is a photonic crystal in one dimension:

The wave equation is:

$$\frac{c^2}{\epsilon(x)} \frac{\partial^2 E}{\partial x^2} = \frac{\partial^2 E}{\partial t^2} \quad (389)$$

With

$$\epsilon(x+a) = \epsilon(x) \quad (390)$$

one finds for the Fourier expansion

$$\epsilon^{-1}(x) = \sum_{m=-\infty}^{\infty} \kappa_m \exp\left(i \frac{2\pi m}{a} x\right) \quad (391)$$

According to Bloch's theorem it is

$$E(x, t) = u_k(x) \exp\{i(kx - \omega_k t)\} \quad (392)$$

with a periodic  $u_k(x)$ .

Fourier expansion results in

$$E(x, t) = \sum_{m=-\infty}^{\infty} E_m \exp\left\{i\left(k + \frac{2\pi m}{a}\right)x - i\omega_k t\right\} \quad (393)$$

For simplicity we assume that only the term  $m = 0$  and  $m = \pm 1$  in the expansions are relevant, i.e.

$$\epsilon^{-1}(x) \approx \kappa_0 + \kappa_1 \exp\left(i \frac{2\pi}{a} x\right) + \kappa_{-1} \exp\left(-i \frac{2\pi}{a} x\right) \quad (394)$$

Inserting into the wave equation 389 provides the recursion relation

$$\begin{aligned} & \kappa_1 \left\{k + \frac{2(m-1)\pi}{a}\right\}^2 E_{m-1} + \kappa_{-1} \left\{k + \frac{2(m+1)\pi}{a}\right\}^2 E_{m+1} \\ & \approx \left\{ \frac{\omega_k^2}{c^2} + \kappa_0 \left(k + \frac{2m\pi}{a}\right)^2 \right\} E_m \end{aligned} \quad (395)$$

For  $m = 0$  it is:

$$E_0 \approx \frac{c^2}{\omega_k^2 - \kappa_0 c^2 k^2} \left\{ \kappa_1 \left(k - \frac{2\pi}{a}\right)^2 E_{-1} + \kappa_{-1} \left(k + \frac{2\pi}{a}\right)^2 E_1 \right\} \quad (396)$$

And for  $m = -1$  it is:

$$E_{-1} \approx \frac{c^2}{\omega_k^2 - \kappa_0 c^2 (k - 2\pi/a)^2} \left\{ \kappa_1 \left( k - \frac{4\pi}{a} \right)^2 E_{-2} + \kappa_{-1} k^2 E_0 \right\} \quad (397)$$

In case of  $k \approx \pi/a$  and  $\omega_k^2 \approx \kappa_0 c^2 k^2$  (close to the boundary of the Brillouin zone) only the terms  $E_0$  and  $E_{-1}$  dominate in the expansion of  $E(x, t)$ .

If only these are considered, one derives a set of coupled equations:

$$(\omega_k^2 - \kappa_0 c^2 k^2) E_0 - \kappa_1 c^2 \left( k - \frac{2\pi}{a} \right)^2 E_{-1} = 0 \quad (398)$$

$$-\kappa_{-1} c^2 k^2 E_0 + \left\{ \omega_k^2 - \kappa_0 c^2 \left( k - \frac{2\pi}{a} \right)^2 \right\} E_{-1} = 0 \quad (399)$$

The set of equations has a non-trivial solution if the determinant of the coefficients vanishes.

The solutions are:

$$\omega_{\pm} \approx \frac{\pi c}{a} \sqrt{\kappa_0 \pm |\kappa_1|} \pm \frac{ac}{\pi |\kappa_1|} \left( \kappa_0^2 - \frac{|\kappa_1|^2}{2} \right) (k - \pi/a)^2 \quad (400)$$

thus, there are no modes between

$$\frac{\pi c}{a} \sqrt{\kappa_0 - |\kappa_1|} < \omega < \frac{\pi c}{a} \sqrt{\kappa_0 + |\kappa_1|} \quad (401)$$

*A bandgap occurs!*

The bandgap vanishes if  $|\kappa_1| = 0$ . In case of  $|\kappa_1| \neq 0$  modes with  $k \approx \pi/a$  and  $k \approx -\pi/a$  are mixed. Figures 207 and 208 illustrate the emerging of a bandgap and the dispersion relation of a one-dimensional Bragg structure for various differences of the index of refraction:

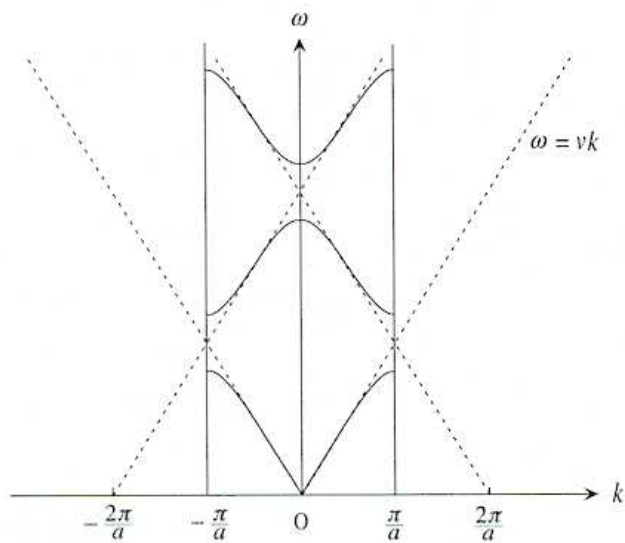


Figure 207: Emerging of a bandgap. [from Sakoda "Optical Properties of Photonic Crystals"]

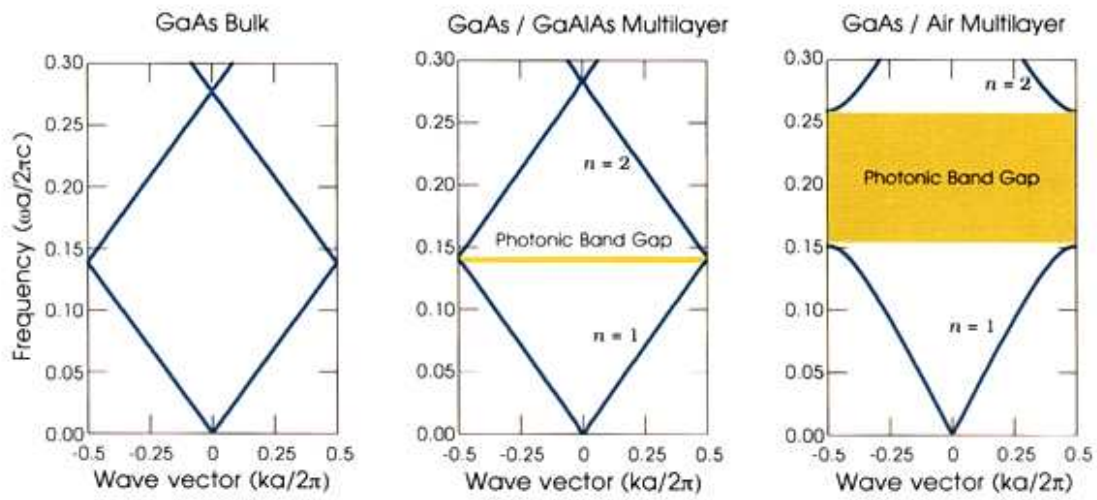


Figure 208: Dispersion relation for a Bragg structure with different dielectric constants: 13 and 13 (= bulk GaAs, left), 13 to 12 GaAs/AlGaAs (middle) and 13 to 1 GaAs/air. [from Joannopoulos "Photonic Crystals"]

The existence of a bandgap in one direction in no way predicts the existence of a bandgap in another direction.

The following figure 209 shows the calculated band structure of a two-dimensional GaAs structure with periodic air holes:

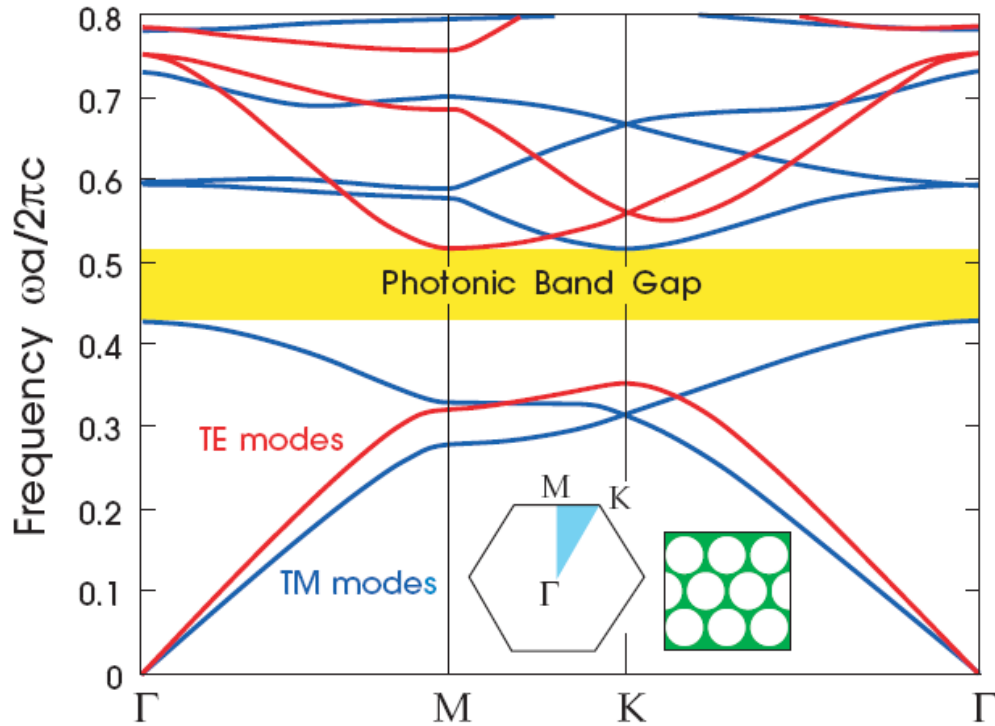


Figure 209: Two-dimensional photonic crystal. [from Joannopoulos "Photonic Crystals"]

In case of an electromagnetic wave (in contrast to a scalar electron wave) the polarization of the field has to be taken into account. The band structure is different for different polarizations.

If a three-dimensional bandgap structure can exist at all was initially unclear. In 1990 the diamond structure was suggested by the group of Soukoulis [K. M. Ho et al. Phys. Rev. Lett. 65, 3152 (1990)] which indeed has a full bandgap. 1991 the group of Yablonovitch realized the first fcc-structure with a full bandgap [E. Yablonovitch et al., Phys. Rev. Lett. 67, 2295 (1990)]. The following figures 210 and 211 show the structure (Yablonovite) and its band structure:

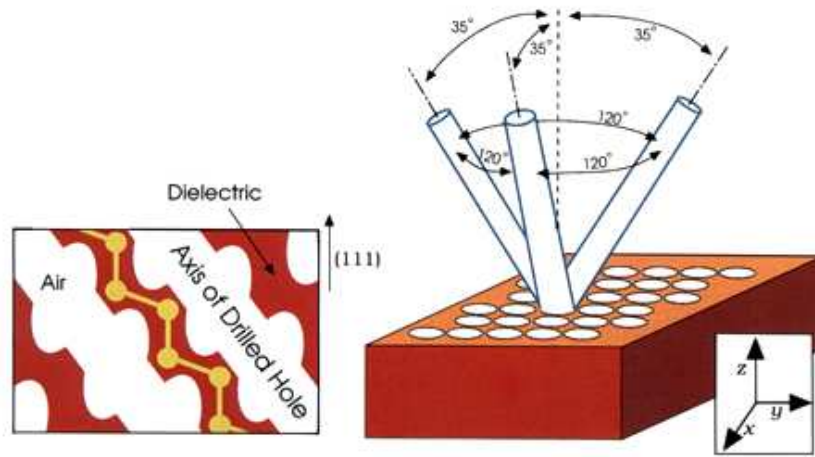


Figure 210: Method to realize Yablonovite. [from Joannopoulos "Photonic Crystals"]

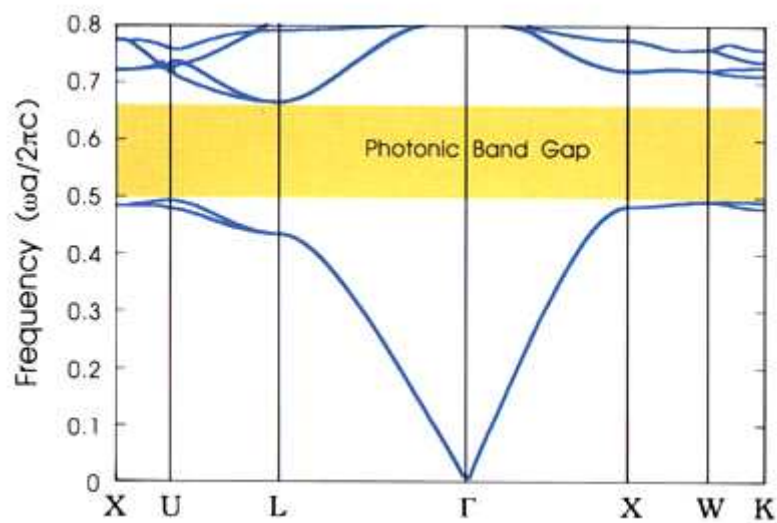


Figure 211: Existence of a bandgap in all three directions in Yablonovite. [from Joannopoulos "Photonic Crystals"]

Apart from the existence of the bandgap itself (applications are discussed below) the modification of the dispersion relation in photonic crystals is of particular importance.

The group velocity is

$$v_g = \frac{\partial \omega}{\partial k} \quad (402)$$

From the dispersion relations above it can be seen that there are bands with a very shallow slope over a rather wide range. This means that there is a *slow group velocity* and thus a longer interaction time of light and matter in such a material. This results in an enhancement of non-linear effects, e.g. frequency conversion or mixing.

Additionally the so-called *phase matching* (conservation of momentum) in frequency conversion is facilitated as the k-vector has to be conserved except for a reciprocal lattice vector:

$$k_{initial} = k_{final} + G \quad (403)$$

This enhances the efficiency of frequency conversion.

#### 8.4 Realizations of photonic crystals

The main difficulty when fabricating photonic crystals is to realize a three-dimensional, periodic, and defect-free modulation of the index of refraction. Therefore, first 3-D photonic crystals with a complete bandgap were fabricated in the microwave domain. There the required periods are on the order of cm to mm.

Photonic crystals in the infrared through the visible are nowadays produced by the following methods:

##### **Direct nanostructuring by electron-beam lithography and etching:**

This method was developed in chip-technology. First periodic structures are written with the help of an electron-beam on a photoresist. Then, the resist is hard-backed and used as an etch mask, or a metal mask is produced via the lift-off technique. Subsequently, etching is performed to imprint the structure in the substrate material.

This approach is particularly suited for two-dimensional structures, such as *photonic crystal membranes*. The following figures 212 and 213 show the fabrication principle and an example of a SiN membrane for bandgaps in the visible. Light confinement in the third dimension is obtained via ordinary total internal reflection:

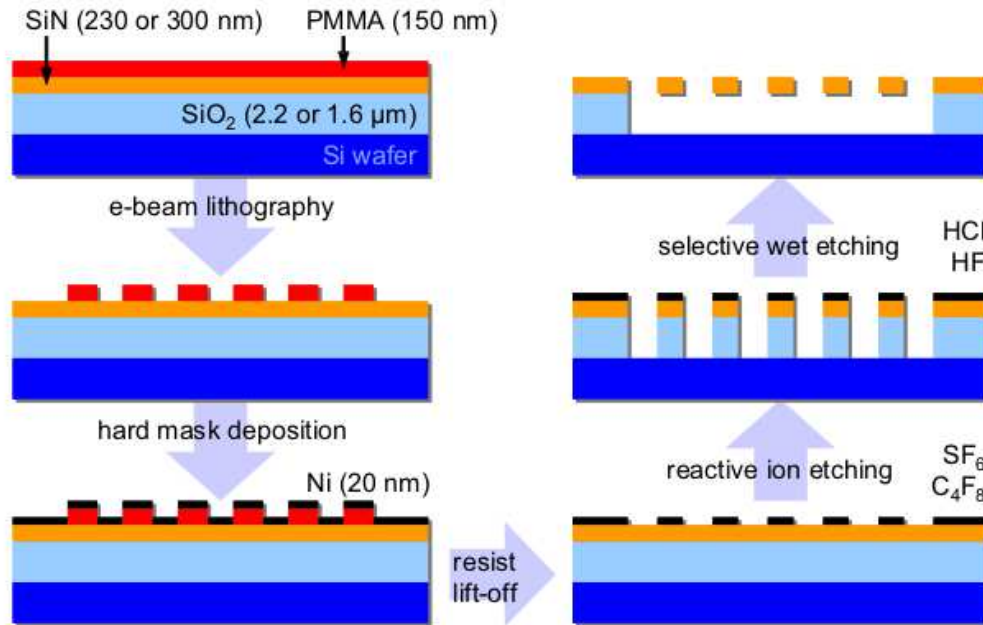


Figure 212: Fabrication of a SiN photonic crystal membrane structure. E-beam writing, developing, metal deposition, lift-off, reactive ion etching, and wet etching are applied sequentially.

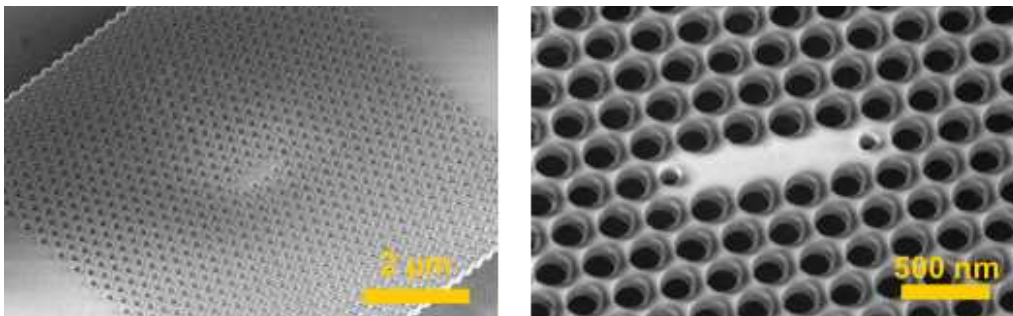


Figure 213: SEM images of a suspended SiN photonic crystal membrane structure.

### Mikromachining:

With two-dimensional suspended structures three-dimensional structures can be assembled directly. A precise positioning of the layers with respect to each other is crucial.

Figures 214 and 215 show lattices which were piled on top of each other with  $90^\circ$  rotation ('woodpile structure'). The exact positioning is facilitated with micrometer sized beads placed in small dents.

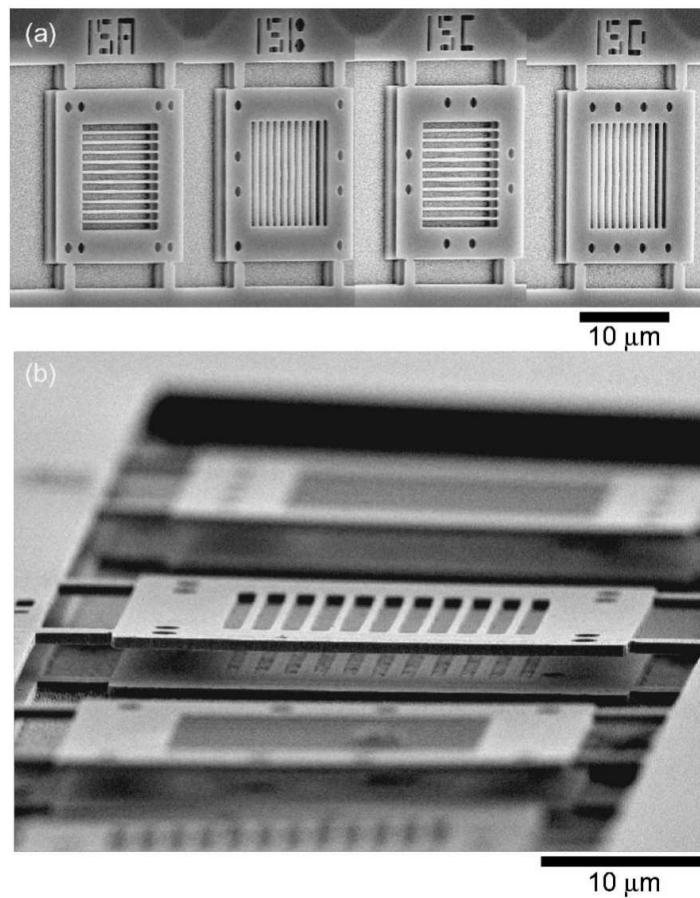


Figure 214: Freely suspended two-dimensional structures. 'Microbeads' are placed in dents to facilitate positioning. [from Aoki et al., Appl. Phys. Lett. 81, 3122 (2002)]

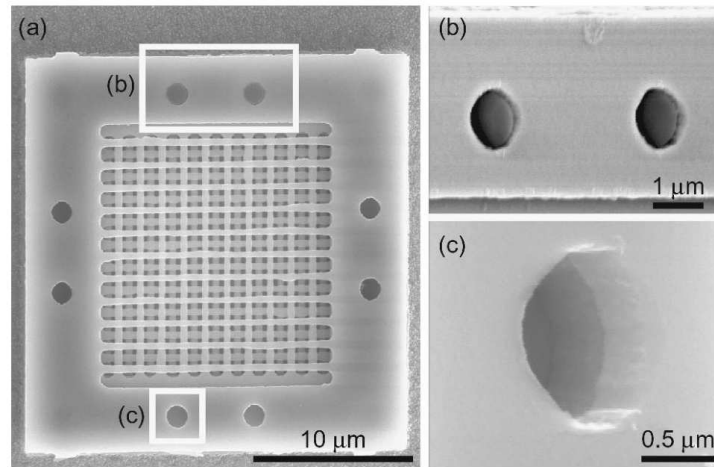


Figure 215: Detailed image of an assembled woodpile structure. [from Aoki et al., Appl. Phys. Lett. 81, 3122 (2002)].

**Self organization:**

The most challenging photonic crystal structures are three-dimensional structures. A completely different approach relies on self-organization of colloidal particles into periodic lattices.

Figure 216 shows a nearly defect free crystal formed out of spherical polymer particles.

Unfortunately, it can be shown that three-dimensional crystals formed by spherical polymer or glass particles can not provide a full bandgap.

*Inversion* of the structure provides a solution to the problem:

- a) Fabrication of a colloidal crystal, e.g. with sub- $\mu$  polymer beads.
- b) Infiltration of the crystal with another material, e.g.  $TiO_2$
- c) Etching of the polymer beads.

The inverted structure (e.g., in an opal lattice in figures 217 and 218) can have a full bandgap:

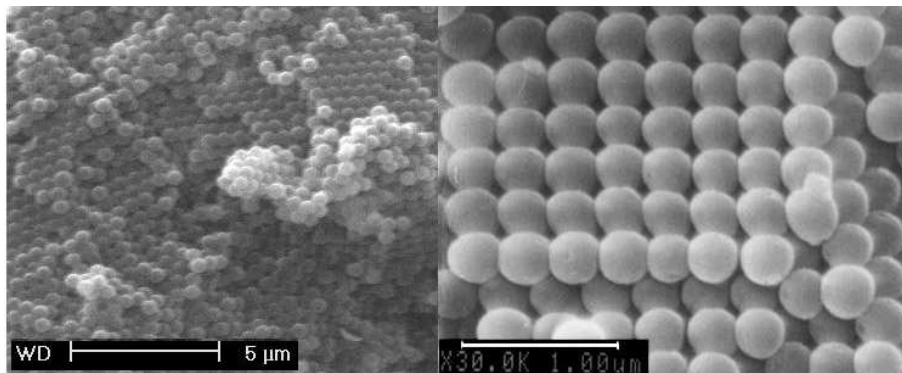


Figure 216: SEM image of a colloidal crystal.

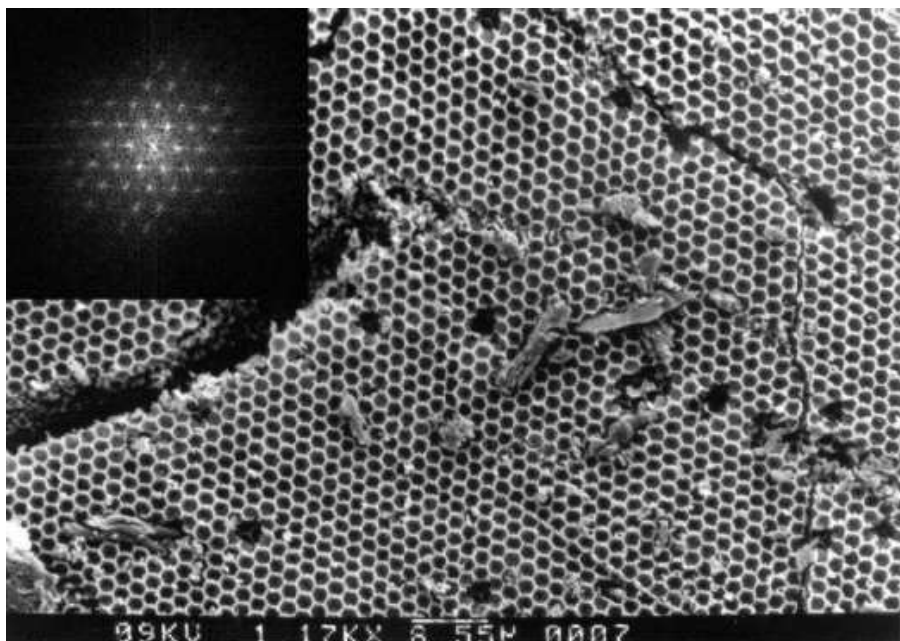


Figure 217: Inverted opal structure. The inset show an x-ray diffraction pattern. [from Wijnhoven et al., Chem. of Mat. Sci., 13, 4486 (2001)]

**Direct laser writing:**

A method that allows to fabricate larger photonic crystals also in three dimensions is direct laser writing (DLW). The method relies on *two-photon polymerization* of suitable polymers and proceeds as follows:

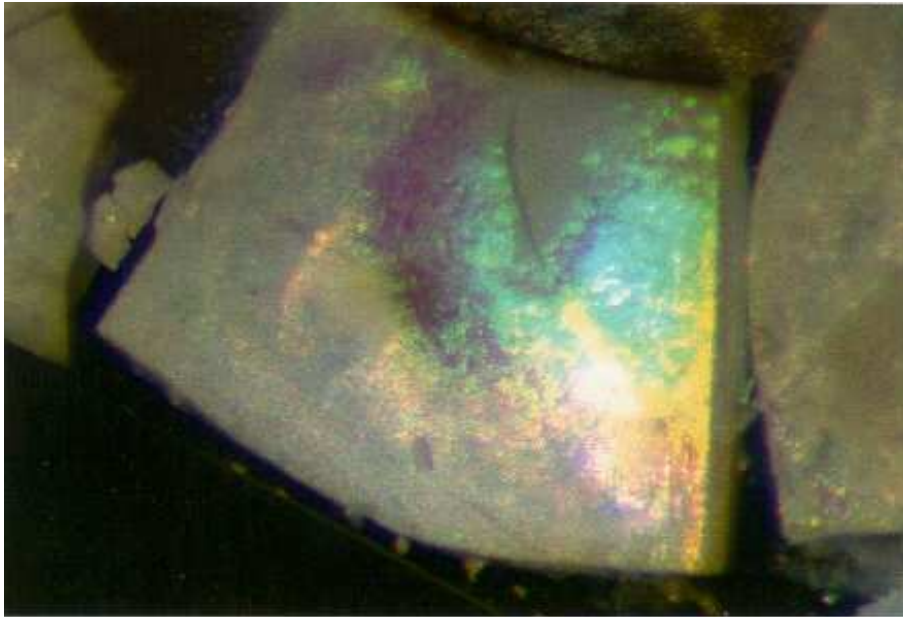


Figure 218: Bragg reflection of white light from an inverted opal structure. [from Wijnhoven et al., Chem. of Mat. Sci., 13, 4486 (2001)]

- Photoresist samples (e.g., the commercially available polymer SU-8) are prepared by spin-coating on microscope cover slides (typical thickness of several  $10\ \mu\text{m}$ ).
- To write photonic crystal structures into these films pulsed Ti:sapphire laser beams of typically a few tens of nanojoules of single pulse energy are coupled into a high-NA oil immersion objective. The resist (polymer) is unaffected by the 800 nm wavelength light, but two-photon absorption may occur and 'develops' the resist. The probability for this to occur is proportional to the intensity squared. This allows a three-dimensional patterning as illustrated in figure 219.
- The sample is placed on a three-axis piezoelectric scanning stage, and a personal computer controls the scanning operation of the piezo and synchronizes its movement with the output of the laser system.
- Finally, the exposed sample is post-baked at about  $65^\circ$  to  $95^\circ$  for several minutes, and developed in an SU-8 developer, resulting in a positive image of the scanned pattern.

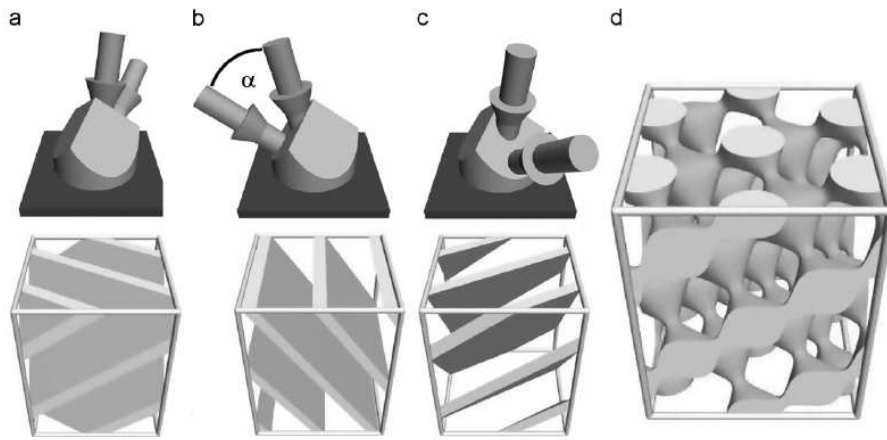


Figure 219: Illustration of the multiple-exposure scheme with the beams coupled into the resist through a corner-cube prism. a) to c) The resist is sequentially exposed to three two-beam interference patterns, only differing in a rotation about a three-fold axis. Each individual exposure would result in a lamellar structure as shown below. By varying the angle  $\alpha$  between the two beams in each pair while maintaining the bisector, the lattice constant can be varied conveniently. d): Resulting three-dimensional simple cubic structure after accumulating the three exposures a) to c). [from Busch et al., Phys. Rep. 444, 101 (2007)]

- It is important to note that the structure can also be used as a template or preform, i.e., another material can be infiltrated (possibly with a higher index of refraction) in order to fabricate an inverted structure with a full bandgap.

The following figure 220 shows a three-dimensional photonic crystal structure fabricated by DLW. Obviously, the defect rate is very low. Also DLW offers enormous flexibility regarding the structure's morphology and material (when used as template).

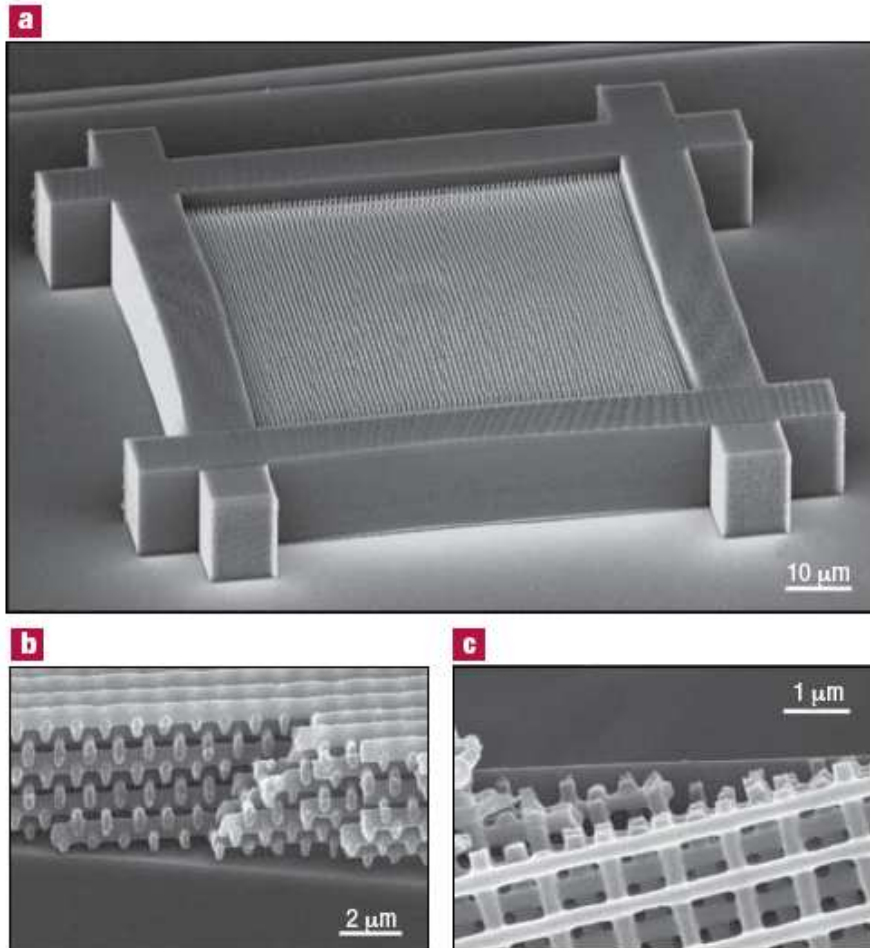


Figure 220: Three-dimensional photonic crystals fabricated by DLW. a) Structure with 40 layers and a massive wall that prevents bending and reduces distortions due to polymer shrinkage during polymerization, completely fabricated by DLW. b) Side and c) top view of a different broken sample with 12 layers. [from Deubel et al., *Nature Mat.* 3, 444 (2004)]

**Realization of photonic crystal structures in nature:**

It has been discovered that photonic crystal structures also occur in nature.

The following figure 221 shows the photo of the seamouse, which lives about 1-2 km at the ocean bed. The seamouse is covered with hairs or spines.



Figure 221: Picture of aphroditidae or seamouse (length 15-20 cm) and close-up of spines.

Similar as in the photonic opal structure the spines reflect various colors when illuminated with white light:

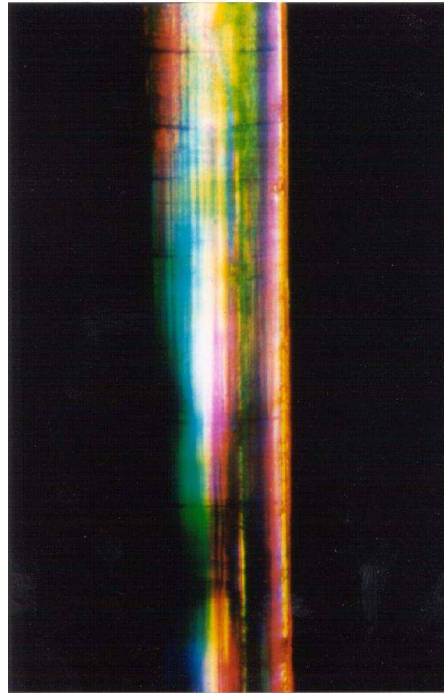


Figure 222: Colors when illuminating a spine of the seamouse with white light.

The reason for the colors is apparent when looking at a cross-cut through a spine by an SEM. The spine actually is a two-dimensional photonic crystal:

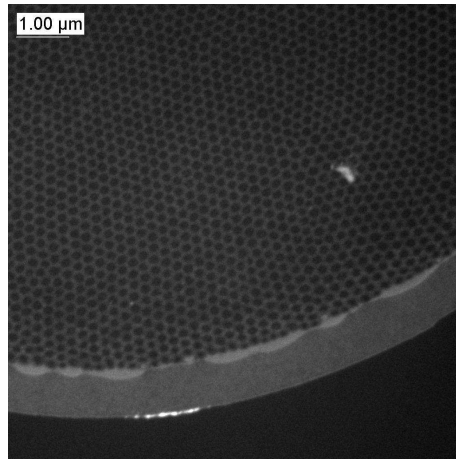


Figure 223:

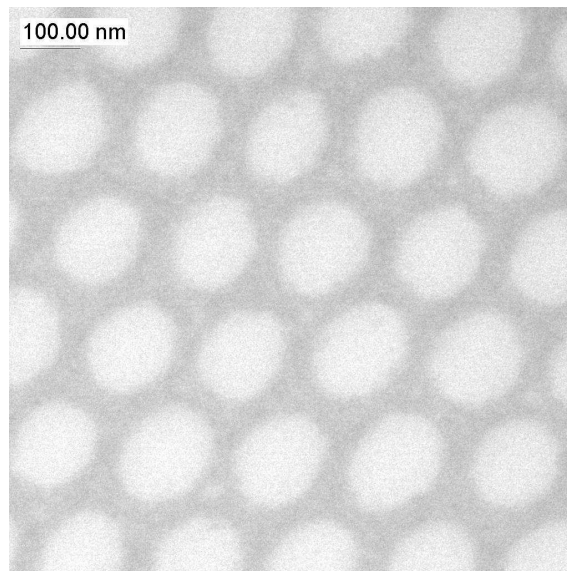


Figure 224: SEM image of a cross-cut through the spine of a seahorse.

The purpose of this advanced structure is not completely clear, but the bright colors are of evolutionary relevance, possibly to attract food or to chase away enemies.

## 8.5 Defects in photonic crystals

As shown above, in photonic crystals there are forbidden frequency gaps (bandgaps) for light. Light cannot propagate and is reflected from the photonic crystal.

If *defects* are implanted in a perfect photonic crystal, then there exist allowed *defect states* in the bandgap. In the spatial domain light is localized close to the defects. This is in analogy to defect states or impurity atoms in the solid state, e.g., in semiconductor materials.

The following figure 225 shows defects in the Yablonovite structure:

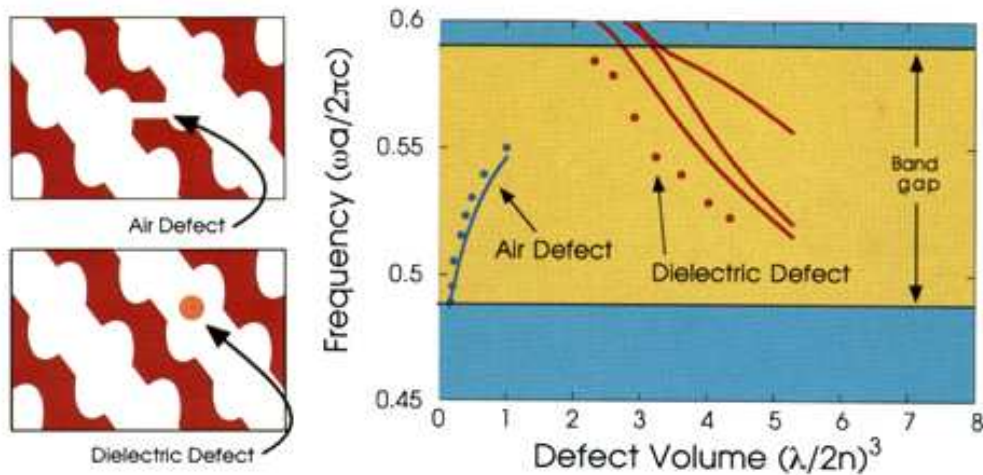


Figure 225: Defect modes in Yablonovite as a function of the defect size. [from Joannopoulos "Photonic Crystals"]

A simulation of the localized electric fields in the vicinity of a defect (see figure 226) demonstrates the strong localization of light:

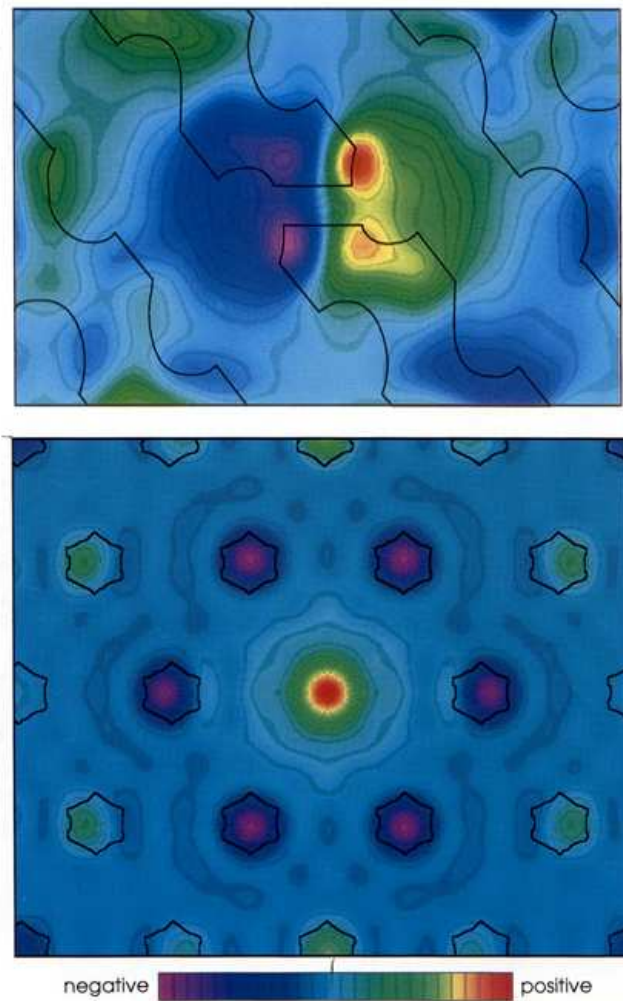


Figure 226: Field strength at an *air defect* in Yablonoivite. Top: Strength of the magnetic H-field, bottom: strength of the electric D-field (in another cross-section through the crystal). [from Joannopoulos "Photonic Crystals"]

The examples above show zero-dimensional or point-like defects in a three-dimensional structure. Light is confined to a very small volume (on the order of  $\lambda^3$ ).

A point-like defect in a photonic crystal represents an *optical microresonator* as light can be trapped efficiently. Another example of a defect in a one-dimensional structure has been discussed above, i.e., the Bragg-resonator. With the help of de-

fects in photonic crystals resonators with a fundamentally small *mode volume* can be fabricated. A small mode volume is essential for the enhancement of quantum electrodynamic effects as will be discussed in a later chapter. As we will see there the electric field per photon is inversely proportional to the mode volume.

Of particular practical importance are one-dimensional defects in two-dimensional structures, e.g., membranes.

Light with a wavelength matched to the defect mode can propagate only along the defect.

**One dimensional defects act as waveguides capable to direct light with tightest confinement!**

The following figure 227 shows a numerical simulation:

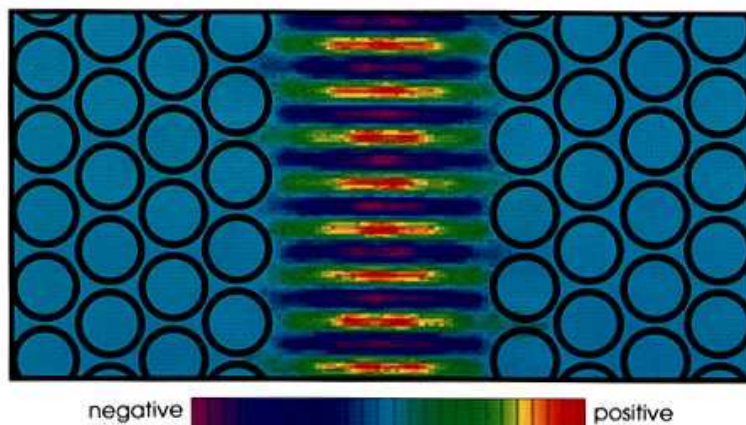


Figure 227: Waveguiding along a one-dimensional defect in a two-dimensional photonic crystal. [from Joannopoulos "Photonic Crystals"]

Waveguiding in photonic crystals relies on a completely different mechanism compared to ordinary waveguides (e.g., optical fibers) where total internal reflection is utilized. Light can be reflected and thus guided independent of the incidence angle.

For this reason there is no critical angle and in principle **light can be guided "around the corner"**.

The following figure 228 shows the simulated intensity distribution in a 90° bend in a waveguide structure.

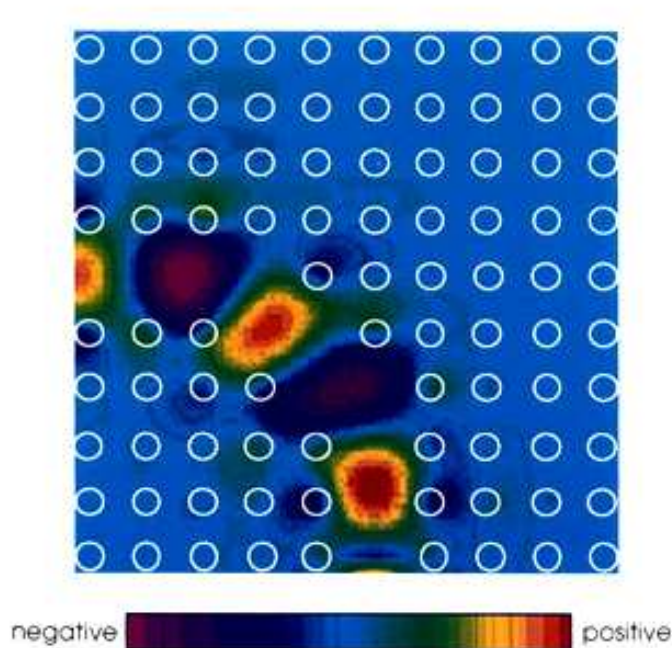


Figure 228: Waveguiding 'around the corner' in a photonic crystal waveguide. [from Joannopoulos "Photonic Crystals"]

In addition to the confined waveguiding also the propagation properties (dispersion, group velocity dispersion, etc.) can be strongly modified in a photonic crystal structure. *Slow light* and *optical buffering* has been suggested.

The following figure 229 shows real-space measurements of pulse propagation in photonic waveguide.

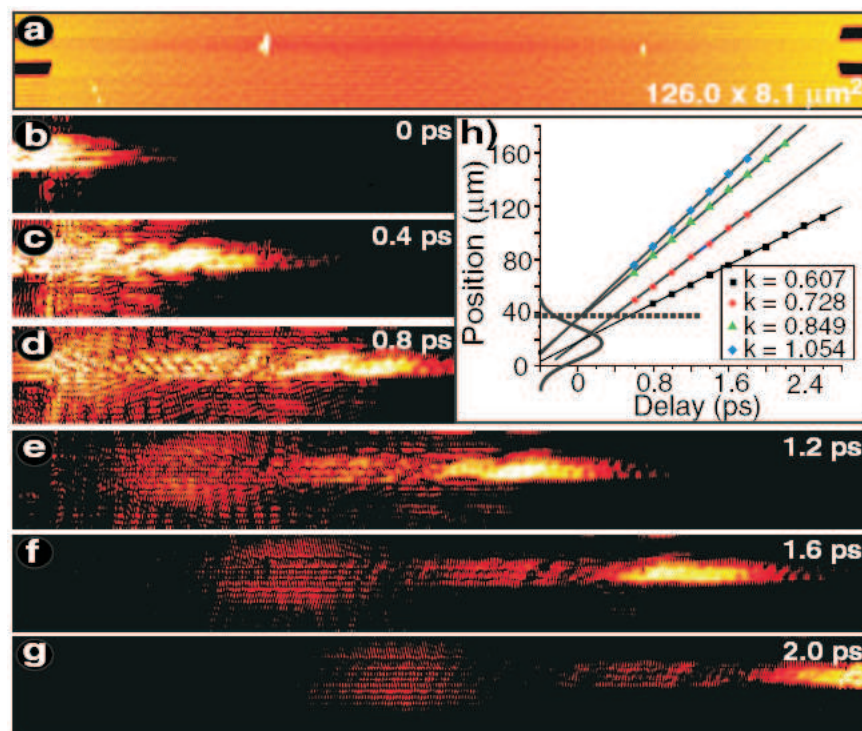
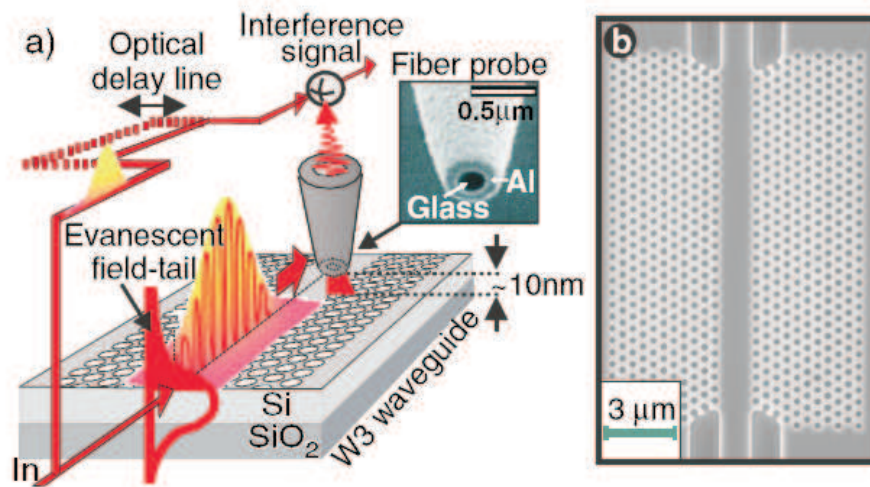


Figure 229: Top: (a) Schematic representation of a pulse tracking experiment. The evanescent field of a propagating pulse is picked up by a metal coated fiber probe with a subwavelength-sized aperture and interferometrically mixed with light from a reference branch. Measurements are done by raster scanning the optical probe across the structure at a constant height ( $<10$  nm). (b) Top view of the PhCW under study; Bottom: A time-resolved NSOM measurement. (a) Topographic image of the structure. (b) to (g) The optical amplitude in the waveguide for different reference times. It is apparent that pulses with different modal distributions and group velocities are excited. (h) The measured position of the center of mass for pulses with different modal distributions (and different wave vectors) as a function of the delay time. [from Gersen, et al. Phys. Rev. Lett. 94, 073903 (2005)]

## 8.6 Applications of photonic crystals

Photonic crystals have found their way to fundamental research as well as to 'true' applications. In the following we list a few topics which are presently investigated:

1. **Integrated optics and passive optical elements:**

The tight confinement of light may allow integrated optical elements, such as waveguides, beam splitters, couplers, mirrors, etc. with much smaller dimensions. In particular two-dimensional structures are appropriate.

2. **Mikroresonators and microlasers:**

Photonic crystals allow the realization of smallest possible optical resonators for microlasers with ultra-low thresholds. Several configurations for photonic crystal lasers have been demonstrated.

Additionally, the enhancement of the intensity and the far stronger interaction of the confined light with any kind of material makes photonic crystals ideal candidates for optical sensing devices. The possibility of high integrability is particularly rewarding.

3. **Modification of spontaneous emission:**

Photonic crystals can strongly modify the spontaneous emission properties of emitters, both the overall rate as well as the direction of emission. Applications in optical antennae, lasers, and LEDs are feasible.

4. **Tunable photonic crystals:**

The bandgap in photonic crystals can be modified by mechanical deformation or active modification of the index of refraction (e.g., by infiltrated liquid crystals). Tunable resonances may be used in optical filters or in modulators.

5. **Enhancement of non-linear optical effects:**

The slow group velocity and the tailoring of dispersion and group velocity dispersion finds application in non-linear optics. Phase-matching can be optimized, and the mentioned intensity enhancement can strongly support frequency conversion, frequency mixing, and optical switching.

Photonic crystal fibers have been used in *frequency-comb generation* and in generation of bright white light for optical coherence tomography.

6. **New dyes:**

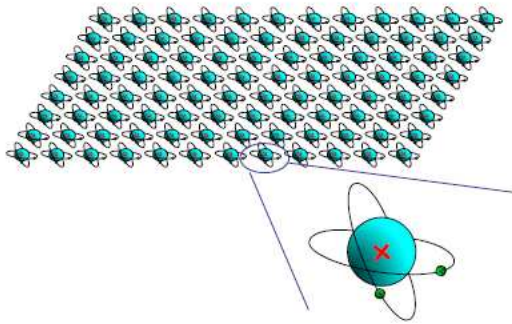
A seemingly trivial, but nevertheless commercially attractive application, are novel dye pigments for colors or the cosmetic industry.

## 8.7 Metamaterials

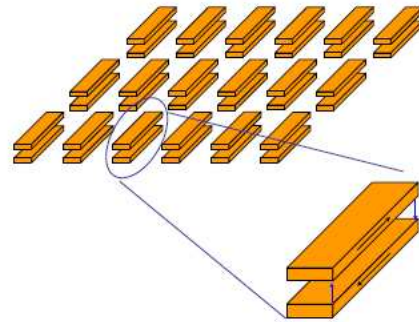
Photonic crystals are one example where nano-structuring can be utilized to change the optical properties of a material. Whereas the typical structure size in photonic crystals is still on the order of the optical wavelength, the concept can be generalized to much smaller structures (see figure 230).

*Materials modified by structuring on a length scale below the optical wavelength and with thereby novel properties which can be described in terms of effective macroscopic parameters ( $\epsilon$ ,  $\mu$ ,  $n$ , etc.) are called **metamaterials**.*

**$\mu\epsilon\tau\alpha$  = meta = beyond (Greek)**



**A natural material with its atoms**



**A metamaterial with artificially structured "atoms"**

Figure 230: Concept of metamaterials. [from homepage V. M. Shalaev, Purdue Univ.]

### 8.7.1 Negative index of refraction

Metamaterials can have unusual properties, which do not occur in natural materials. Of particular interest are the possibilities to generate negativities in  $\epsilon$  and  $\mu$ .

Since

$$n = \pm\sqrt{\epsilon\mu} \quad (404)$$

also negativities in  $n$  are possible.

Pioneering theoretical work in **negative index of refraction** or in **negative index material (NIM)** was performed by Veselago (1968) and Pendry (1999).

The following figure 231 shows the unusual refraction at an interface with a negative index of refraction  $n$ .

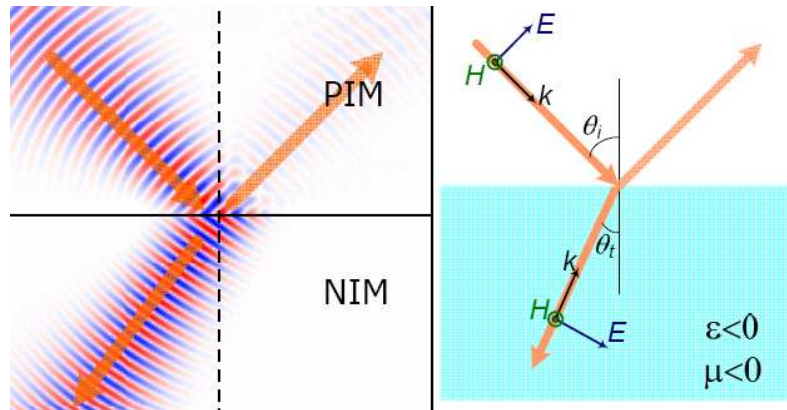


Figure 231: Ray optics picture (right) and numerical simulation of negative refraction at a planar interface. [from homepage V. M. Shalaev, Purdue Univ.]

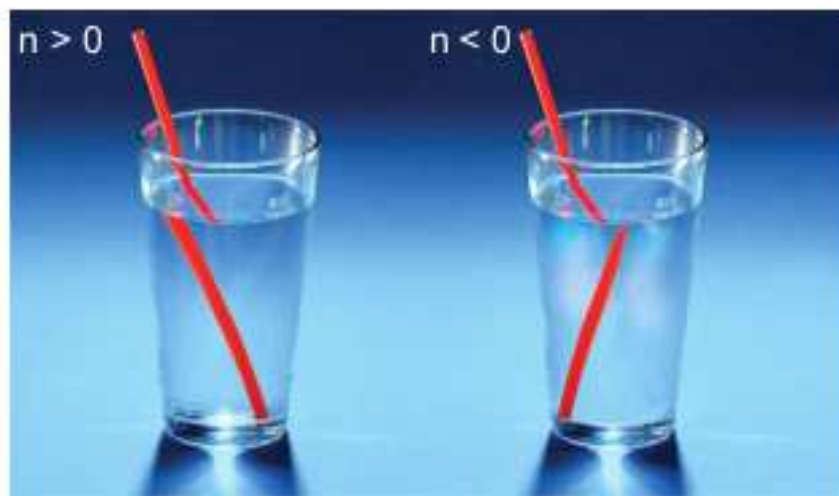


Figure 232: Image of glass of water with ordinary water and a possible liquid with negative index of refraction.

In a NIM material both  $\epsilon$  and  $\mu$  are negative. In such materials the wavevector  $k$  of a plane electromagnetic wave forms a left-handed triplet with the electric  $E$  and

magnetic  $H$  field vectors, i. e. the Poynting vector  $S$  is antiparallel to  $k$ . This has also coined the name *left-handed material*.

In general the index of refraction  $n$ , the electric and magnetic permittivity  $\epsilon$  and  $\mu$ , respectively, can have an imaginary component. The notation is as follows:

$$n = n' + in'' \quad (405)$$

$$\epsilon = \epsilon' + i\epsilon'' \quad (406)$$

$$\mu = \mu' + i\mu'' \quad (407)$$

The real part of  $n$  is responsible for dispersion, whereas the imaginary part accounts for absorption. A figure of merit of a material with negative index of refraction is that the ratio  $|n'|/n''$  is large, i.e. there is a strong refraction without absorption.

The special phenomenon of negative refraction can be observed even if not both  $\epsilon$  and  $\mu$  are negative. Strictly speaking the condition for negative  $n < 0$  is:

$$\epsilon'|\mu| + \mu'|\epsilon| < 0 \quad (408)$$

One often subdivides the two cases:

- **single-negative material:**  $n < 0$  and  $\epsilon' < 0$ , but  $\mu' > 0$  where  $|n'|/n''$  is low.
- **double-negative material:**  $n < 0$  and  $\epsilon' < 0$  and  $\mu' < 0$  where  $|n'|/n''$  is large.

### 8.7.2 Application of NI materials

An intriguing application of a NIM is obvious when following rays which are refracted at a planar slab of NI material.

It is apparent that a NIM can form a *perfect lens* (Pendry 1999) without any aberrations. It is not necessary to mention the breakthrough which such a material may represent.

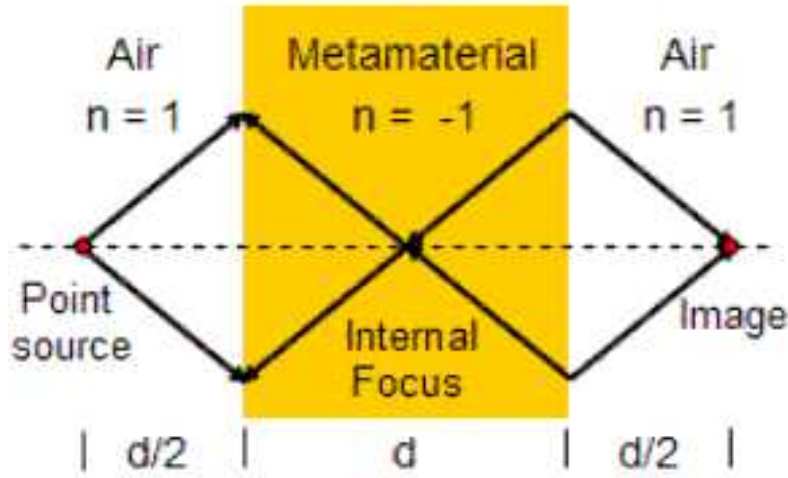


Figure 233: Principle of a perfect lens using a slab of NI material.

As was discussed already in the theory chapter an imaging system typically has a finite resolution. The reason is that information of small spatial features, i.e., with large spatial frequencies, does not propagate, but is contained only in the evanescent fields. The condition for the  $z$ -component of a propagating field propagating in  $z$ -direction is:

$$k_z = \sqrt{k_0^2 - k_y^2 - k_x^2} \quad \text{and} \quad k_t = \sqrt{k_x^2 + k_y^2} < k_0 \quad (409)$$

Evanescent fields decay exponentially in ordinary material and are not available in the far field.

This is different in NIM (see figure 234) as equation 409 does not apply. Exponential fields are 're-covered' in a NIM! Thus, a *superresolution* can be expected.

Superresolution has caused significant debate, however, first experimental demonstrations exist. We will provide examples at the end of the following subsection.

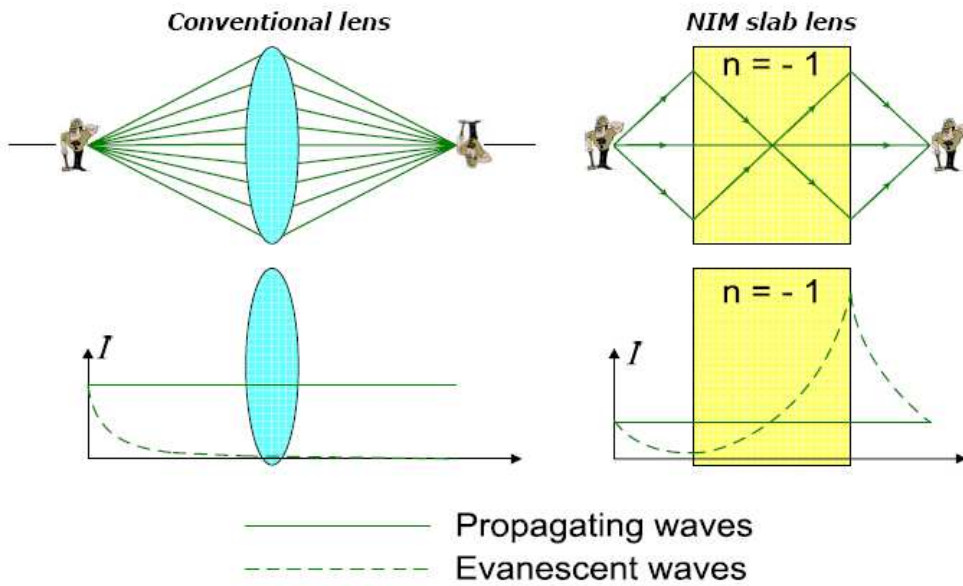


Figure 234: Imaging with an ordinary lens (left) and a superlens (right). Note that evanescent fields are enhanced in a NI material.

### 8.7.3 Fabrication of NI materials

Specific optical properties are not available in natural materials. Figure 235 is a quadrant-plot of negative/positive  $\epsilon$  and  $\mu$ .

Obviously in order to realize materials with pronounced negative  $\mu$  metamaterials are required. Electric materials have been studied for a longer time with respect to shifting down the plasmon frequency in order to have large negativities of  $\epsilon$  at longer wavelengths.

Pendry found in 1996 (PRL 76, 4773) that a metallic mesostructure can be described as a continuous medium, but with a very low plasmon frequency (see figure 236).

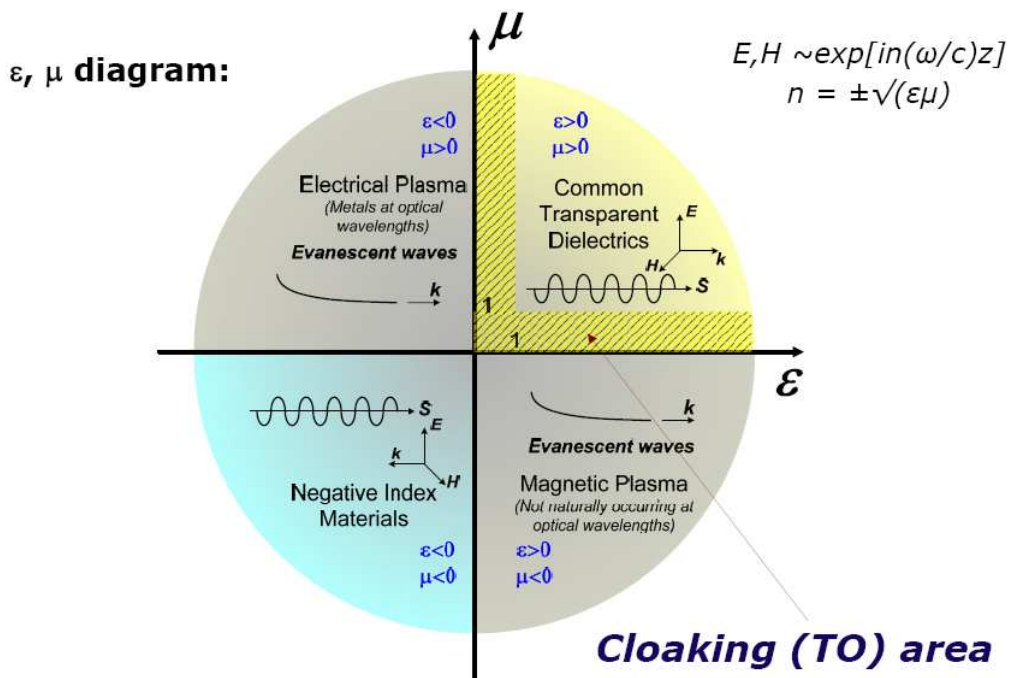


Figure 235:  $\epsilon$ - $\mu$ -diagram. [from homepage V. M. Shalaev, Purdue Univ.]

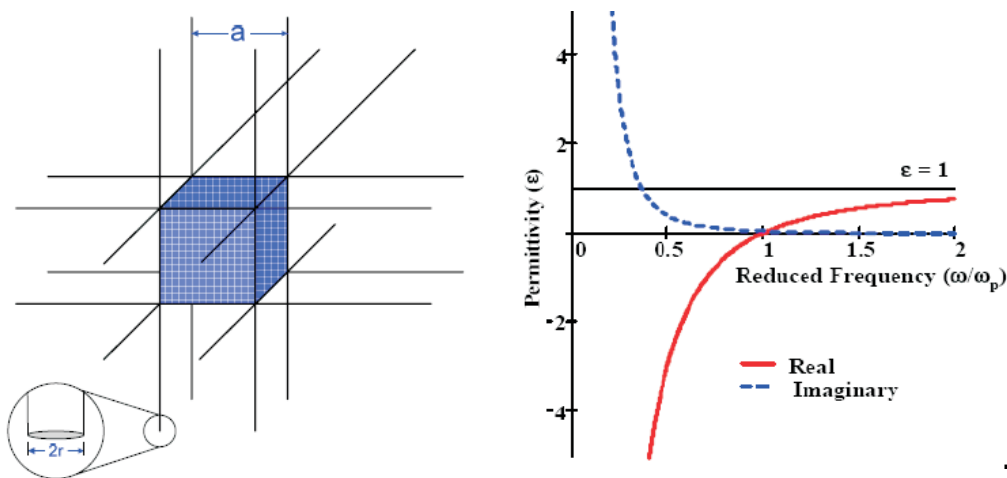


Figure 236: Left: Schematics of the metal wire structure in a cubic lattice; Right: Calculated real and imaginary part of  $\epsilon$ . [Pendry et al., PRL 76, 4773]

The electric permittivity of the metal wire structure can be described as:

$$\epsilon = \epsilon' + i\epsilon'' = 1 - \frac{\omega_p^2}{\omega (\omega + i\epsilon_0 a^2 \omega_p^2 / \pi r^2 \sigma)} \quad (410)$$

where  $\sigma$  is the conductivity of the metal and with the modified plasmon frequency:

$$\omega_p = \frac{2\pi c^2}{a^2 \ln(a/r)} \quad (411)$$

Consequently the route to design a material with large negative magnetic permeability is to fabricate structures with a magnetic resonance (typically the magnetic interaction is by a factor of the hyperfine structure squared smaller than the electric interaction).

The design idea by Pendry is shown in figure 237.

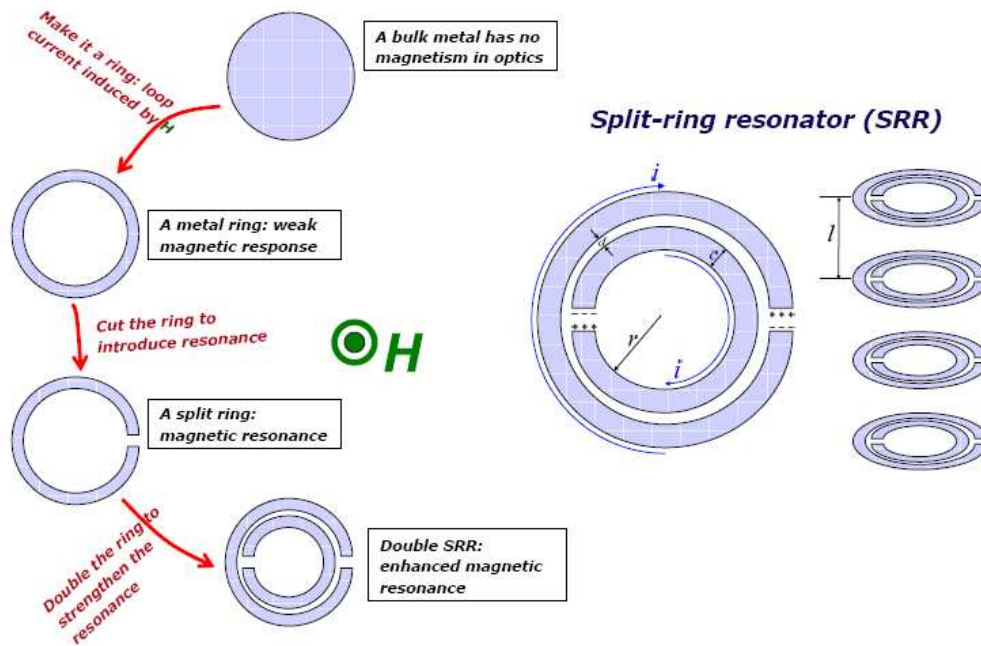


Figure 237: Strategy to implement materials with negative  $\mu$ . [from homepage V. M. Shalaev, Purdue Univ.]

Obviously, the scaling down of structures from the millimetre via micrometer to optical wavelengths is extremely challenging. Also losses become a significant problem at higher frequencies. The following figures 238 and 239 show examples.

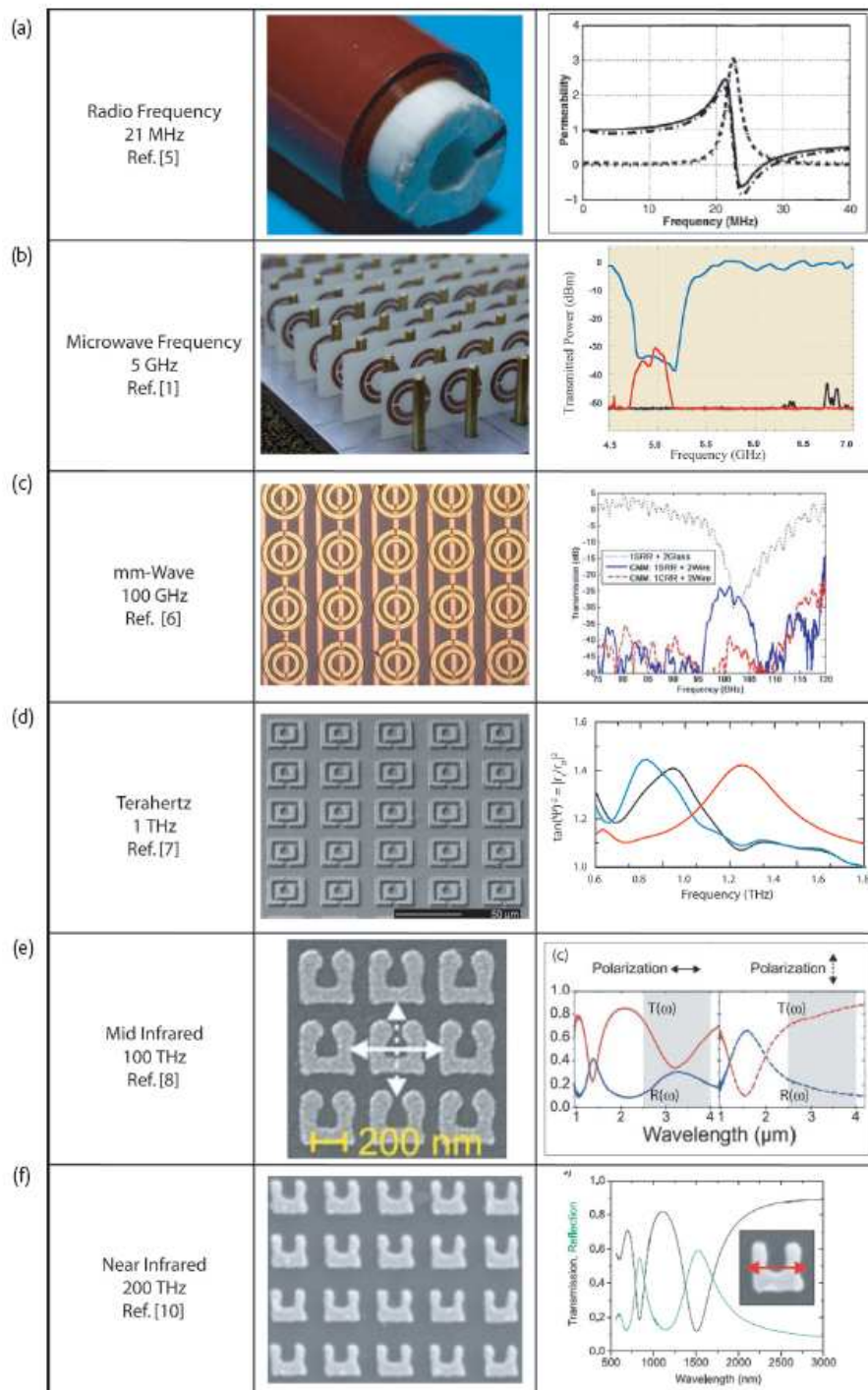


Figure 238: Summary of various magnetic material (MM) structures from RF to near optical frequencies. In the left column the frequency range and a reference is indicated. The middle column shows photos of the MMs, and the third column shows some data detailing the MM response. The top row is an investigation of swiss-roll-type magnetic structures to guide magnetic flux in magnetic resonance imaging machines. The second row is the original work in which NI materials were discovered at microwave frequencies. The third row shows some recent work on MMs at millimeter-wave frequencies. The next column details the first work extending MMs out of the microwave into the terahertz regime. The bottom two columns show further extension of the MM MIR and NIR frequencies. [from Padilla et al., *Materialstoday* 9, 28 (2006)]

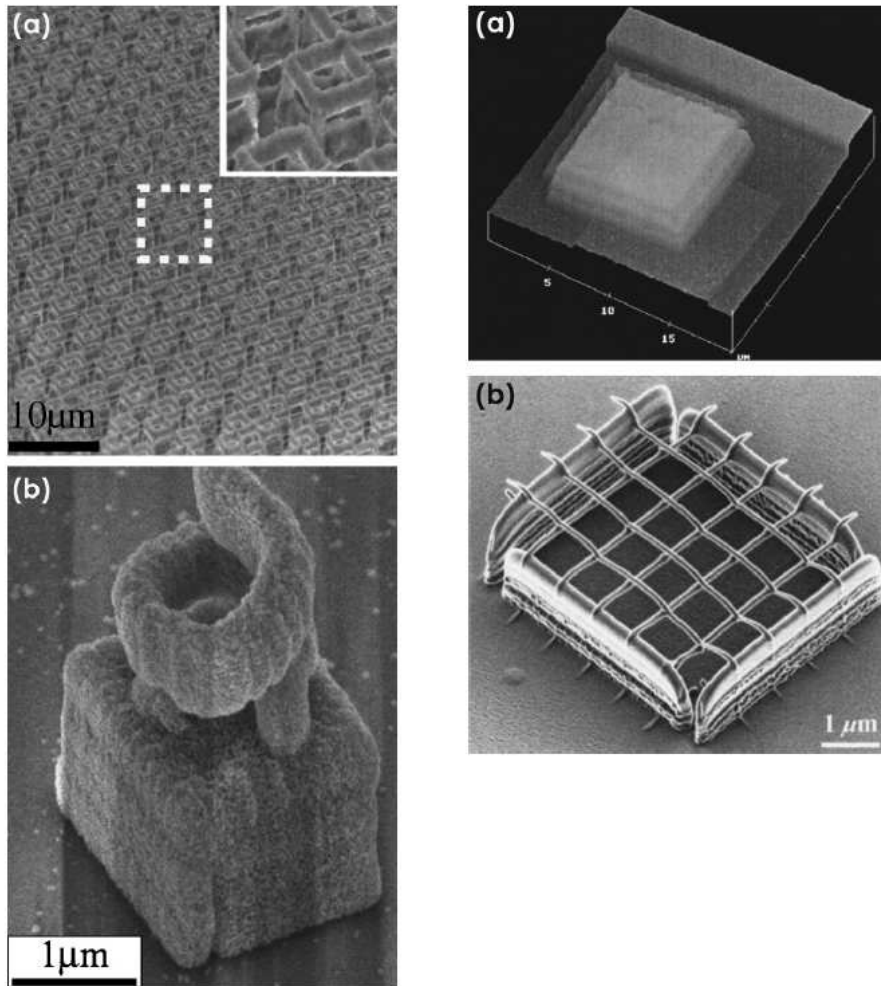


Figure 239: Left column: Scanning electron microscope images of (a) self-standing empty cubic structures (height  $\approx 4.6 \mu\text{m}$ ) connected in pairs and (b) a silver-coated polymer structure composed of a cube ( $2 \mu\text{m}$  in size) holding up a spring (inner diameter  $700 \text{ nm}$ ). The structures are made by a two-photon induced photopolymerization technique (direct laser writing, DLW) combined with electroless plating; Right column: Towards complex 3D structures: (a) atomic force microscope image of a multilayer (AgAuAg) structure prepared by electron-beam exposure of solutions of thiol-capped metal nanoparticles (electron-beam stereolithography process) and (b) scanning ion microscope image of a crossbar circuit structure fabricated by using focused-ion beam chemical vapor deposition (conducting wires contain Ga and W). [from A. Boltasseva and V. M. Shalaev, *Metamaterials* 2, 1-17 (2008)]

Finally, the next figures 240 and 241 as well as figures 242 and 243 show experimental results of the superlens effect with a simple layered silver structure.

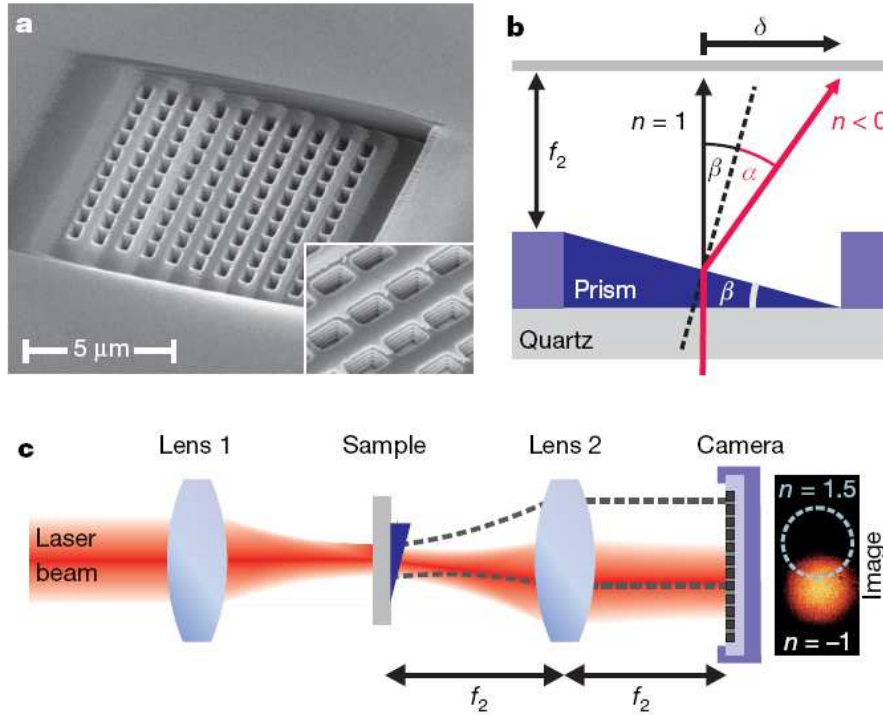


Figure 240: SEM image of NIM prism and schematics of experimental setup. a) SEM image of the fabricated 3D fishnet NIM prism. The inset shows a magnified view with the film layers visible in each hole. b) Geometry diagram of the angle measurement;  $\delta$  corresponds to the position difference of the beam passing through a window in the multilayer structure ( $n = 1$ ) and prism sample. By measuring  $\delta$ , the absolute angle of refraction  $\alpha$  can be obtained. c) Experimental setup for the beam refraction measurement. The focal length of lens 1 is 50 mm and that of lens 2 is  $f_2 = 540$  mm. Lens 2 is placed in a  $2f$  configuration, resulting in the Fourier image at the camera position. [from Valentine et al., Nature 455, 376 (2008)]

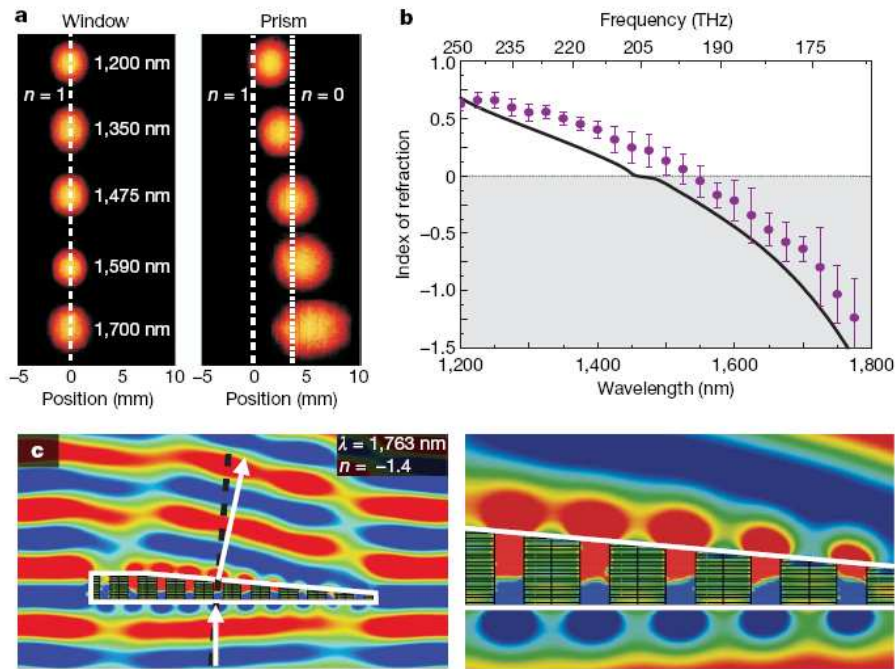


Figure 241: Experimental results and finite-difference time-domain simulations. a) Fourier-plane images of the beam for the window and prism sample for various wavelengths. The horizontal axis corresponds to the beam shift  $\delta$ , and positions of  $n = 1$  and  $n = 0$  are denoted by the white lines. The image intensity for each wavelength has been normalized for clarity. b) Measurements and simulation of the fishnet refractive index. The circles show the results of the experimental measurement with error bars (s.d.,  $n = 4$  measurements). The measurement agrees closely with the simulated refractive index using the RCWA method (black line). c) Left: simulation of the in-plane electric field component for the prism structure at 1,763 nm, showing the phase front of the light. Negative-phase propagation resulting from the negative refractive index leads to negative refraction angle as measured by the beam shift in the experiment. Right: magnified plot of the field distribution in the prism. [from Valentine et al., Nature 455, 376 (2008)]

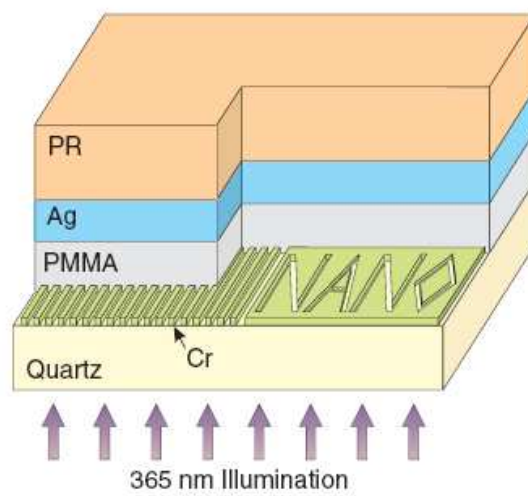


Figure 242: Structure for an optical superlensing experiment. The embedded objects are inscribed onto the 50- nm-thick chrome (Cr); On the left is an array of 60- nm-wide slots of 120 nm pitch, separated from the 35-nm-thick silver film by a 40-nm PMMA spacer layer. The image of the object is recorded by the photoresist on the other side of the silver superlens. [from Fang et al., Science 308, 534 (2005)]

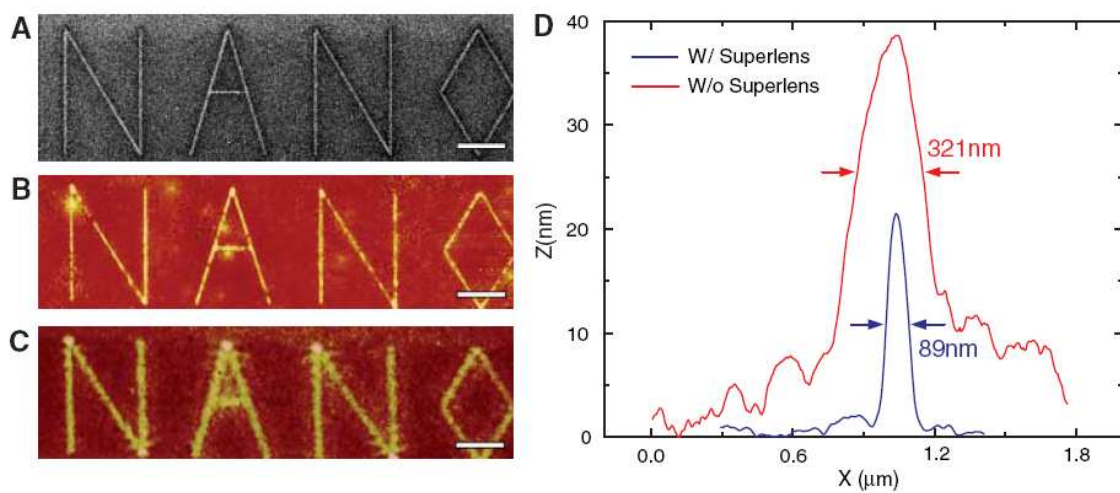


Figure 243: An arbitrary object NANO was imaged by silver superlens. (A) FIB image of the object. The linewidth of the NANO object was 40 nm. Scale bar in (A) to (C), 2 μm. (B) AFM of the developed image on photoresist with a silver superlens. (C) AFM of the developed image on photoresist when the 35-nm-thick layer of silver was replaced by PMMA spacer as a control experiment. (D) The averaged cross section of letter A shows an exposed line width of 89 nm (blue line), whereas in the control experiment, a diffraction-limited full width at halfmaximum line width of  $321 \pm 10$  nm (red line) was measured. [from Fang et al., *Science* 308, 534 (2005)]